Inorg. Chem. **2008**, *47*, 2897−2908

Tuning the Redox Properties of Manganese(II) and Its Implications to the Electrochemistry of Manganese and Iron Superoxide Dismutases

Martin Sjödin,[†] Jessica Gätjens,[†] Leandro C. Tabares,[†] Pierre Thuéry,[‡] Vincent L. Pecoraro,[§] and Sun Un*[,†]

Service de bioénergétique biologie structurale et mécanismes, CNRS URA 2096, Institut de Biologie et de Technologies de Saclay, CEA Saclay, 91191 Gif-sur-Yvette, France, Service de chimie moléculaire, CNRS URA 331, Institut Rayonnement Matière de Saclay, CEA Saclay, 91191 Gif-sur-Yvette, France, and Department of Chemistry, University of Michigan, Ann Arbor, Michigan 48109-1055

Received December 17, 2007

Superoxide dismutases (SODs) catalyze the disproportionation of superoxide to dioxygen and hydrogen peroxide. The active metal sites of iron and manganese superoxide dismutases are structurally indistinguishable from each other. Despite the structural homology, these enzymes exhibit a high degree of metal selective activity suggesting subtle redox tuning of the active site. The redox tuning model, however, up to now has been challenged by the existence of so-called cambialistic SODs that function with either metal ion. We have prepared and investigated two sets of manganese complexes in which groups of varying electron-withdrawing character, as measured by their Hammett constants σ_{Para}, have been introduced into the ligands. We observed that the Mn(III)/Mn(II) reduction potential for the series based on 4′-X-terpyridine ligands together with the corresponding values for the iron-substituted 4′-X-terpyridine complexes changed linearly with σ_{Para}. The redox potential of the iron and manganese complexes could be varied by as much as 600 mV by the 4′-substitution with the manganese complexes being slightly more sensitive to the substitution than iron. The difference was such that in the case where the 4′-substituent was a pyrrolidine group both the manganese and the iron complex were thermodynamically competent to catalytically disproportionate superoxide, making this particular ligand "cambialistic". Taking our data and those available from the literature together, it was found that in addition to the electron-withdrawing capacity of the 4′-substituents the overall charge of the Mn(II) complexes plays a major role in tuning the redox potential, about 600 mV per charge unit. The ion selectivity in Mn and FeSODs and the occurrence of cambialistic SODs are discussed in view of these results. We conclude that the more distant electrostatic contributions may be the source of metal specific enzymatic activity.

Introduction

Manganese is an essential metal for life and plays a central role in a number of important biological processes, such as photosynthesis,[1] the regulation of oxidative stress,[2] and bacterial virulence.[3] In a number of proteins, manganese ions not only have roles as structural centers or sites of Lewis acid catalysis, but are also electrochemically active.[4] Hence, it is surprising that, although many redox potentials of manganese complexes have been measured, there are many fewer studies on how the ligand sphere modulates this important physical property. The ability to control the redox potential is not only important for the function of manganese ions as catalytical centers, but may also participate actively in regulating the activity of a protein. Vance and Miller have suggested that the high level of metal-specific activity in the manganese-iron family of superoxide dismutases (SOD) is due to protein-controlled redox properties of the metal ions.[5]

* To whom correspondence should be addressed. E-mail: sun.un@cea.fr.
† Service de bioénergétique biologie structurale et mécanismes.
‡ Service de chimie moléculaire.
§ University of Michigan.

(1) *Oxygenetic Photosynthesis: The Light Reactions*; Ort, D., Yocum, C. F., Eds.; Kluwer Academic Publishers: Dordrecht, The Netherlands, 1996.
(2) Horsburgh, M. J.; Wharton, S. J.; Karavolos, M.; Foster, S. J. *Trends Microbiol.* **2002**, *10*, 496–501.
(3) Papp-Wallace, K. M.; Maguire, M. E. *Annu. Rev. Microbiol.* **2006**, *60*, 187–209.

10.1021/ic702428s CCC: $40.75
Published on Web 02/14/2008

This family of SODs exhibits a high degree of structural homology, yet when Fe is substituted into MnSOD or Mn into FeSOD, neither reconstituted protein is active.[6] More intriguing is that there exists a subfamily of the Mn−Fe family of SODs that is active with either manganese or iron, the so-called cambialistic type.[7]

SODs are specialized in the depletion of superoxide from the cell through a ping-pong mechanism in which a first molecule of superoxide is oxidized to dioxygen and then a second molecule is reduced to peroxide.[8] This process is mediated by the cyclic reduction and oxidation of the metal cofactor for which the reduction potential of the metal(III)/metal(II) couple in the protein must be between the superoxide reduction and oxidation potentials (0.89 and −0.16 V vs NHE, respectively).[9] The reduction potentials of MnSOD and FeSOD (0.29 and 0.22 V, respectively) are fine-tuned to perform both superoxide reduction and oxidation,[10] while aqueous $Mn(III)(H_2O)_6/Mn(II)(H_2O)_6$ and $Fe(III)(H_2O)_6/Fe(II)(H_2O)_6$ couples that have reduction potentials of 1.54 and 0.77 V, respectively,[11] are suggested to react with $O_2^{\bullet-}$ following a different mechanism.[12]

To obtain a more detailed understanding of how the redox potential of a manganese(II) ion is modulated by its environment, we have synthesized and examined two sets of manganese(II) complexes (Figure 1). The first contains a series of 4′-substituted 2,2′:6′,2″-terpyridine (terpy) ligands. The terpy was chosen since many stable compounds are accessible through simple modification of the ligand periphery. The second set of complexes was based on the ligand *N*,*N*-bis-(2-ethyl-5-methyl-imidazol-4-ylmethyl)aminopropane (biap).[13] Two nitrogen donor atoms derived from the substituted imidazole moieties, which closely mimic histidine residues. The coordination sphere was completed by the tertiary amine nitrogen atom of the biap ligand, as well as two para-substituted benzoic acids and a water molecule (Figure 1). Hence, the biap-based series more closely resembled the active site of SOD.

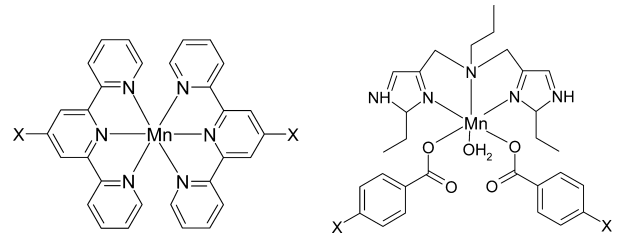

Figure 1. Schematic representation of $Mn(4'\text{-X-terpy})_2^{2+}$ (left) and $Mn(biap)(p\text{-X-bz})_2$ (right). The substituent X was, in order of decreasing Hammett constant σ_{Para} or electron-withdrawing power, Cl, H, CH_3Ph, OH, or pyrrolidine (pyrr) for $Mn(4'\text{-X-terpy})_2^{2+}$ and NO_2, Cl, H, Ph, ^{t}Bu, and CH_3 for $Mn(biap)(p\text{-X-bz})_2$.

In both cases, our intent was to use aromatic ring substitutions to mimic secondary electrostatic/inductive influences of the protein and the basic terpy or biap/benzoic acid moieties to model the primary ligand sphere. To quantify the effects of each substituent, the redox potentials of the manganese complexes were measured and correlated to the Hammett constants (σ_{Para}) for each substituted ligand. This constant gives a quantitative measure of the electron-withdrawing/electron-donating properties of the substituent.[14] Although the Hammett relationship was originally developed to rationalize the effect of substituents on the ionization of benzoic acids in solution,[15] it has been successfully applied to a number of other experiments evaluating the redox chemistry of metal complexes.[16] The sensitivity of the reduction potential to the electron-donating capacity of the substituent within a series of complexes was obtained from the Hammett reaction constant (ρ), which is a dimensionless parameter that is specific for the reaction being followed.[14] In our case, it was defined as the slope of a plot of the reduction potential as a function of the Hammett parameter σ_{Para} per substituent.

The effect of the 4′-substitution on the redox potential of iron and cobalt terpy complexes has recently been investigated by Chambers and co-workers.[16c] They showed that the redox potential of these complexes was linearly related to the Hammett constant of the 4′-substituent. Although not stated, it was clear from their results that those Fe complexes that had the most electron-donating substituents were at least in principle thermodynamically competent to carry out the disproportionation of superoxide. Chambers did point out that the relative effect of the 4′-substituent was greater for the Fe complexes than the corresponding Co complexes; that is, the iron complexes had a larger reaction constant ρ than the corresponding cobalt complexes.

(4) Yocum, C. F.; Pecoraro, V. L. *Curr. Opin. Chem. Biol.* **1999**, *3*, 182–187.
(5) (a) Vance, C. K.; Miller, A.-F. *J. Am. Chem. Soc.* **1998**, *120*, 461–467. (b) Vance, C. K.; Miller, A.-F. *Biochemistry* **2001**, *40*, 13079–13087.
(6) (a) Brock, C. J.; Harris, J. I. *Biochem. Soc. Trans.* **1977**, *5*, 1537–1539. (b) Ose, D. E.; Fridovich, I. *Arch. Biochem. Biophys.* **1979**, *194*, 360–364. (c) Yamakura, F. *J. Biochem.* **1980**, *88*, 191–196. (d) Yamakura, F.; Kobayashi, K.; Ue, H.; Konno, M. *Eur. J. Biochem.* **1995**, *227*, 700–706.
(7) (a) Martin, M. E.; Byers, B. R.; Olson, M. O.; Salin, M. L.; Arceneaux, J. E.; Tolbert, C. *J. Biol. Chem.* **1986**, *261*, 9361–9367. (b) Sugio, S.; Hiraoka, B. Y.; Yamakura, F. *Eur. J. Biochem.* **2000**, *267*, 3487–3495. (c) Tabares, L. C.; Bittel, C.; Carrillo, N.; Bortolotti, A.; Cortez, N. *J. Bacteriol.* **2003**, *185*, 3223–3227.
(8) Whittaker, J. W. In *Metal Ions in Biological Systems, Vol. 37*, Sigel, A., Sigel, H., Eds.; Marcel Dekker: New York, Basel, 2000, *587*; p 611.
(9) Sawyer, D. T.; Valentine, J. S. *Acc. Chem. Res.* **1981**, *14*, 393–400.
(10) Miller, A.-F. In *Handbook of Metalloproteins*; Messerschmidt, A., Huber, R., Wieghardt, K., Paulos, T., Eds.; Wiley and Sons: Chichester, U.K., 2001; Vol. *2*, pp 668–682.
(11) *CRC Handbook of Chemistry and Physics*, 87th ed.; Lide, D. R., Ed.; CRC Press: Boca Raton, FL, 2006; p 2007.
(12) (a) Halliwell, B. *FEBS Lett.* **1975**, *56*, 34–38. (b) Howie, J. K.; Sawyer, D. T. *J. Am. Chem. Soc.* **1976**, *98*, 6698–6700. (c) McClune, G. J.; Fee, J. A.; McCluskey, G. A.; Groves, J. T. *J. Am. Chem. Soc.* **1977**, *99*, 5220–5222. (d) Archibald, F. S.; Fridovich, I. *Arch. Biochem. Biophys.* **1982**, *214*, 452–463.
(13) Bouwman, E.; Douziech, B.; Gutierrez-Soto, L.; Beretta, M.; Driessen, W. L.; Reedijk, J.; Mendoza-Díaz, G. *Inorg. Chim. Acta* **2000**, *304*, 250–259.
(14) Hansch, C.; Leo, A.; Taft, R. W. *Chem. Rev.* **1991**, *91*, 165–195.
(15) Hammett, L. P. *J. Am. Chem. Soc.* **1937**, *59*, 96–103.
(16) For example, see (a) Constable, E. C.; Cargill Thompson, A. M. W.; Tocher, D. A.; Daniels, M. A. M. *New J. Chem.* **1992**, *16*, 855−867. (b) Lewis, E. A.; Lindsay Smith, J. R.; Walton, P. H.; Archibald, S. J.; Foxon, S. P.; Giblin, G. M. P. *J. Chem. Soc., Dalton Trans.* **2001**, 1159–1161. (c) Chambers, J.; Eaves, B.; Parker, D.; Claxton, R.; Ray, P. S.; Slattery, S. J. *Inorg. Chim. Acta* **2006**, *359*, 2400–2406. (d) Fang, Y.-Q.; Taylor, N. J.; Laverdière, F.; Hanan, G. S.; Loiseau, F.; Nastasi, F.; Campagna, S.; Nierengarten, H.; Leize-Wagner, E.; Van Dorsselaer, A. *Inorg. Chem.* **2007**, *46*, 2854–2863.

On the basis of periodic trends, the increase in ρ upon going from cobalt to iron raised the possibility that the manganese complexes would be even more affected by ligand substitution. If true, this could explain, at least in part, how the SODs induce metal-specific activity. Furthermore, this redox behavior could be the basis for the existence of the cambialistic SODs and demonstrate the redox criteria for this subclass to function properly.

To test these ideas, we have examined how the redox potential of manganese(II) depends on the electron-donating properties of substituents in the ligand periphery as quantified by the Hammett parameter σ_{Para} of the substituent. We have focused our attention on para-substituted benzoic acids and 4′-substituted terpyridine ligands to introduce subtle changes in the electronic structure of the related Mn(II) complexes. Periodicity effects were assessed using corresponding iron(II) terpyridine complexes. In addition, we analyzed the manganese crystal structures in detail for substitution effects. High-field EPR spectroscopy was used to monitor the structural integrity and electronic structure of the Mn(II) complexes in frozen solutions and in the crystalline state. These results are presented in a recent communication.[17] Hybrid Hartree–Fock density-functional calculations were used to understand the relationship between the phenomenological observations and the changes in electronic structure of the metal ions induced by substitution in the ligand periphery.

Experimental Section

Abbreviations. Pyr, pyridine; terpy, 2,2′:6′,2″-terpyridine; 4′-Cl-terpy, 4′-chloro-2,2′:6′,2″-terpyridine; 4′-OH-terpy, 4′-hydroxy-2,2′:6′,2″-terpyridine; 4′-CH_3Ph-terpy, 4′-(4-methylphenyl)-2,2′:6′,2″-terpyridine; 4′-pyrr-terpy, 4′-pyrrolidine-2,2′:6′,2″-terpyridine; 4′-DMA-terpy, 4′-(*N*,*N*-dimethylamine)-2,2′:6′,2″-terpyridine.

Materials and Methods. The compounds *N*,*N*-bis-(2-ethyl-5-methyl-imidazol-4-ylmethyl)aminopropane (biap),[13] 4′-pyrrolidine-2,2′:6′,2″-terpyridine,[16c] $[Fe(terpy)_2](PF_6)_2$,[18] $[Fe(4'\text{-Cl-terpy})_2](PF_6)_2$,[16c] $[Fe(4'\text{-OH-terpy})_2](PF_6)_2$,[16c] $[Fe(4'\text{-}CH_3\text{Ph-terpy})_2](PF_6)_2$,[16c] $[Fe(4'\text{-pyrr-terpy})_2](PF_6)_2$,[16c] $[Fe(4'\text{-DMA-terpy})_2](PF_6)_2$,[16a] and $[Mn(terpy)_2](ClO_4)_2$[19] were synthesized as previously described. The composition of the $[Fe(4'\text{-X-terpy})_2](PF_6)_2$ complexes was confirmed by ESI-mass spectrometry and FT-IR spectroscopy. The ligands 2,2′:6′,2″-terpyridine, 4′-chloro-2,2′:6′,2″-terpyridine, 4′-(4-methylphenyl)-2,2′:6′,2″-terpyridine, and 2,6-bis(2-pyridyl)-4(1*H*)-pyridone (4′-hydroxy-2,2′:6′,2″-terpyridine) were purchased from Sigma-Aldrich and ACROS organics. Chemicals for syntheses and analyses were of analytical grade and used as received without any further purification, unless stated otherwise. Elemental analyses were carried out using a Perkin-Elmer 2400 Series II Analyzer. Infrared spectra were recorded as KBr pellets on a Perkin-Elmer Spectrum BX-FTIR spectrometer. Electrospray-ionization mass spectrometry (ESI-MS) spectra were recorded using a Micromass LCT time-of-flight mass spectrometer with electrospray and APCI, coupled with a Waters 1525 Binary HPLC pump.

Syntheses. *Caution! Although we encountered no problems, organic metal perchlorates are potentially explosive and should be handled only in small quantities with care!*

1. $[Mn(4'\text{-X-terpy})_2](ClO_4)_2$. Following procedures described in the literature,[19] the $[Mn(4'\text{-X-terpy})_2](ClO_4)_2$ complexes were isolated from the reaction of $Mn(ClO_4)_2\cdot 6H_2O$ and the respective ligand. In general, a solution (slurry) of the appropriate ligand (0.6 mmol) in 12 mL of hot ethanol was added to a solution of $Mn(ClO_4)_2\cdot 6H_2O$ (0.25 mmol) in 5 mL of distilled water. In most cases, the immediate formation of a precipitate was observed. The yellow mixture was stirred for 2 h and then filtered. The yellow precipitate was washed with small amounts of ethanol and diethyl ether. To increase the yields, the filtrate solution was further concentrated. Yellow single crystals suitable for X-ray diffraction analysis were grown by diffusion of diethyl ether into a dilute solution of the respective compound in acetonitrile. Single crystals of $[Mn(4'\text{-pyrr-terpy})_2](ClO_4)_2$ were grown by slow evaporation of an acetonitrile solution at room temperature.

2. $[Mn(biap)(p\text{-X-bz})_2]$. Following a modified procedure of Reedijk and co-workers,[20] a solution of the biap ligand (0.5 mmol) in 1 mL of methanol was added to a solution of $Mn(ClO_4)_2\cdot 6H_2O$ (0.5 mmol) in 1 mL of methanol. After 10 min of stirring under nitrogen, a solution of the corresponding benzoic acid derivative (1.0 mmol in 1 mL of H_2O, X = H, sodium salt; 1.0 mmol in 1 mL of CH_3CN, addition of 10 drops of triethylamine, X = Cl, CH_3, Ph, ^{t}Bu, NO_2). In most cases, the formation of a white precipitate was observed. Usually, about 10 mL of H_2O was added in order to increase the yield. The precipitate was filtered, washed with small amounts of water, and dried. Colorless single crystals suitable for X-ray diffraction analysis were grown by slow evaporation of a dilute solution of the respective compound in ethanol/DMSO.

The manganese complexes were characterized by elemental analysis, FT-IR spectroscopy, ESI mass spectrometry, and X-ray diffraction analysis. A summary of the results obtained for the standard analyses is presented in Table 1.

Crystal Structures. The crystallographic data and a listing of important bond lengths and angles are presented in the Supporting Information together with details on the structure determination.

Electron Paramagnetic Resonance (EPR). The locally built high-field EPR spectrometer has been described elsewhere.[21] The polycrystalline samples were prepared by finely grinding the material and dispersing it in mineral oil followed by freezing in liquid nitrogen. Free powders could not be used since they tended to orient in the high magnetic field utilized in the experiments. Frozen solution samples were the same as those used for electrochemical measurements (see below). All the spectra were obtained at 4 K under nonsaturating conditions with 20 G modulation. Simulations of the spectra were obtained using standard second-order perturbation expansions of the $S = 5/2$ spin Hamiltonian. Transition probabilities were calculated to first order, and thermal population effects were determined using Boltzmann's equation. The zero-field parameters were obtained by fitting of the spectra using standard conjugate-gradient techniques.

Electrochemistry. Electrochemical measurements were carried out at ambient temperature in a 0.1 M tetrabutylammonium hexafluorophosphate ($TBAPF_6$) (Fluka electrochemical grade) ac-

(17) Gätjens, J.; Sjödin, M.; Pecoraro, V. L.; Un, S. *J. Am. Chem. Soc.* **2007**, *129*, 13825–13827.
(18) Hathcock, D. J.; Stone, K.; Madden, J.; Slattery, S. J. *Inorg. Chim. Acta* **1998**, *282*, 131–135.
(19) (a) Rao, J. M.; Hughes, M. C.; Macero, D. J. *Inorg. Chim. Acta* **1976**, *18*, 127–131. (b) Morrison, M. M.; Sawyer, D. T. *Inorg. Chem.* **1978**, *17*, 333–337.
(20) Warzeska, S. T.; Miccichè, F.; Mimmi, M. C.; Bouwman, E.; Kooijman, H.; Spek, A. L.; Reedijk, J. *J. Chem. Soc., Dalton Trans.* **2001**, 3507–3512.
(21) Un, S.; Dorlet, P.; Rutherford, A. W. *Appl. Magn. Reson.* **2001**, *21*, 341–361.

Table 1. Analytical Data for the Complexes

X	elemental analysis (%)	FT-IR (KBr, cm^{-1})	ESI-MS *m/z* (positive mode)
		$[Mn(4'\text{-X-terpy})_2](ClO_4)_2$	
Cl	calcd for $C_{30}H_{20}Cl_4MnN_6O_8$ (found) C 45.65 (45.73), H 2.55 (2.47), N 10.65 (10.60)	1594, 1478, 1400, 1246, 1090, 792, 622	589 (3%, $[Mn(4'\text{-Cl-terpy})_2]^{2+}$)
CH_3Ph	calcd for $C_{44}H_{34}Cl_2MnN_6O_8 \cdot CH_3CN$ (found) C 58.67 (59.56), H 3.96 (4.01), N 10.41 (10.23)	1612, 1602, 1546, 1476, 1400, 1246, 1088, 790, 622	701 (3%, $[Mn(4'\text{-MePh-terpy})_2]^{2+}$)
OH	calcd for $C_{30}H_{22}Cl_2MnN_6O_{10}$ (found) C 47.89 (48.07), H 2.95 (3.12), N 11.17 (11.19)	1620, 1602, 1585, 1480, 1429, 1400, 1302, 1222, 1121, 1107, 1020, 792, 621	552 (15%, $[Mn(4'\text{-OH-terpy})_2]^{2+}$)
pyrr	calcd for $C_{38}H_{36}Cl_2MnN_8O_8 \cdot 0.5CH_3CN$ (found) C 53.28 (53.37), H 4.30 (4.45), N 13.54 (13.42)	2863, 1613, 1570, 1519, 1473, 1447, 1399, 1121, 1095, 1023, 793, 621	758 (20%, $[Mn(4'\text{-pyrr-terpy})_2(ClO_4)]^+$)
		$[Mn(biap)(p\text{-X-bz})_2]$	
NO_2	calcd for $C_{31}H_{39}MnN_7O_9$ (found) C 52.54 (52.26), H 5.55 (5.40), N 13.84 (13.79)	3158, 2957, 2929, 2872, 1620, 1583, 1524, 1456, 1388, 1344,1107, 1013, 723	524 (15%, $[Mn(biap)(p\text{-}NO_2\text{-bz})]^+$)
Cl	calcd for $C_{31}H_{39}MnN_5O_5Cl_2$ (found) C 54.16 (53.30), H 5.72 (5.78), N 10.19 (10.19)	3195, 3136, 2961, 2922, 2872, 1631, 1599, 1553, 1462, 1390, 1090, 1013, 774	513 (100%, $[Mn(biap)(p\text{-Cl-bz})]^+$)
H	calcd for $C_{31}H_{40}MnN_5O_5.H_2O$ (found) C 58.58 (58.40), H 6.66 (6.50), N 11.02 (11.05)	3062, 2922, 2870, 1627, 1600, 1550, 1463, 1390, 1065, 717	479 (100%, $[Mn(biap)(bz)]^+$)
Ph	calcd for $C_{43}H_{49}MnN_5O_5 \cdot 2H_2O \cdot 0.5CH_3CN$ (found) C 63.87 (64.04), H 6.64 (6.45), N 9.31 (9.43)	3176, 3120, 3058, 3026, 2964, 2930, 2872, 1630, 1596, 1576, 1536, 1458, 1398, 1102, 1078, 1046, 752	555 (35%, $[Mn(biap)(p\text{-Ph-bz})]^+$), 753 (1%, $[Mn(biap)(p\text{-Ph-bz})_2]^+$)
^{t}Bu	calcd for $C_{39}H_{57}MnN_5O_5.2.5H_2O$ (found) C 60.37 (60.26), H 8.05 (7.59), N 9.03 (8.90)	3126, 2964, 2902, 2868,1610, 1592, 1542, 1460, 1398, 1106, 1080, 1044, 788, 714	535 (100%, $[Mn(biap)(p\text{-}^t\text{Bu-bz})]^+$)
CH_3	calcd for $C_{32}H_{42}MnN_5O_5$ (found) C 60.85 (60.78), H 6.70 (7.07), N 11.09 (10.88)	3188, 3132, 3062, 2959, 2932, 2873, 1620, 1596, 1548, 1460, 1395, 1080, 1064, 1044, 767	>493 (100%, $[Mn(biap)(p\text{-}CH_3\text{-bz})]^+$)

etonitrile (Sigma Aldrich HPLC grade) solution with an analyte concentration of 2 mM if not stated otherwise. The solvent was dried over 8–12 mesh molecular sieves (Aldrich), and the analyte solution was purged with argon and kept under argon atmosphere during measurement. A conventional three-electrode system connected to a CH-Instruments electrochemical workstation (CHI660C) was used. The reference electrode (Ag/AgCl in saturated KCl_{aq}), that was kept in a separate compartment filled with electrolyte solution and connected to the analyte solution by a glass frit, was calibrated against ferrocene[22] using the same conditions as for the sample after each measurement series. A commercial glassy carbon electrode with a diameter of 3 mm was used as working electrode, and a freshly annealed platinum wire served as auxiliary electrode. The glassy carbon working electrode was polished on 0.3 μm Alumina (Buehler) before each series of measurement or, when required due to adsorption of the analyte, after each measurement. Cyclic voltammograms (CV) were typically recorded at a scan rate of 0.1 V s^{-1}. Unless noted otherwise, the reported data are from reproducible voltammograms from multiple consecutive scans centered on the recorded redox process or processes. For differential pulse measurements (DPV) the sample was excited with a 50 mV pulse with duration of 60 ms. A equilibration time of 140 ms was used, and the current was sampled for 20 ms before and at the end of the pulse. The measurement parameters for square wave voltammetry (SWV), the pulse amplitude and frequency, were set to 25 mV and 15 Hz, respectively. Cyclic voltammograms were analyzed with the software provided by CH-Instruments, while DP- and SW-voltammograms were processed in Origin by fitting the votammetric peaks to a Gaussian. All reported data are from the average of the oxidative and the reductive DPV peaks.

(22) Gritzner, G.; Kuta, J. *Pure Appl. Chem.* **1984**, *56*, 461–466.

Quantum Chemical Calculations. Calculations were carried out with the Gaussian 03 (Revision B.05) package. All structures were geometry optimized using the B3LYP hybrid density functional and LANL2DZ basis-set.[23] The Natural Bond Orbital (NBO) analysis and Mulliken charges and spin densities were obtained from subsequent calculation using the optimized structures and the 6–311 basis set.[23]

Results

Figure 2 shows XSHELL[24] representations of the $[Mn(4'\text{-X-terpy})_2]^{2+}$ cations. Perchlorate counterions, solvent molecules, and hydrogen atoms were omitted for clarity. Detailed examination of the crystallographic data showed that the 4′-substitution did affect the structure of the $[Mn(4'\text{-X-terpy})_2]^{2+}$ complex cations. By the comparison of these crystallographic data with the geometry-optimized structures using hybrid Hartree–Fock density functional calculations based on the

(23) (a) Becke, A. D. *J. Chem. Phys.* **1993**, *98*, 5648–5652. (b) Lee, C.; Yang, W.; Parr, R. G. *Phys. Rev. B* **1988**, *37*, 785–789. (c) Vosko, S. H.; Wilk, L.; Nusair, M. *Can. J. Phys.* **1980**, *58*, 1200–1211. (d) Stephens, P. J.; Devlin, F. J.; Chabalowski, C. F.; Frisch, M. J. *J. Phys. Chem.* **1994**, *98*, 11623–11627. (e) Dunning,, T. H., Jr.; Hay, P. J. In *Modern Theoretical Chemistry*; Schaefer, H. F., III, Ed.; Plenum: New York, 1976; Vol. *3*, pp 1–28. (f) Hay, P. J.; Wadt, W. R. *J. Chem. Phys.* **1985**, *82*, 270–283. (g) Wadt, W. R.; Hay, P. J. *J. Chem. Phys.* **1985**, *82*, 284–298. (h) Hay, P. J.; Wadt, W. R. *J. Chem. Phys.* **1985**, *82*, 299–310. (i) Krishnan, R.; Binkley, J. S.; Seeger, R.; Pople, J. A. *J. Chem. Phys.* **1980**, *72*, 650–654. (j) Wachters, A. J. H. *J. Chem. Phys.* **1970**, *52*, 1033–1036. (k) Hay, P. J. *J. Chem. Phys.* **1977**, *66*, 4377–4384.

(24) XSHELL, *SHELXTL version 5.1.*, **1998**, Bruker AXS.

(25) Oshio, H.; Spiering, H.; Ksenofontov, V.; Renz, F.; Gütlich, P. *Inorg. Chem.* **2001**, *40*, 1143–1150.

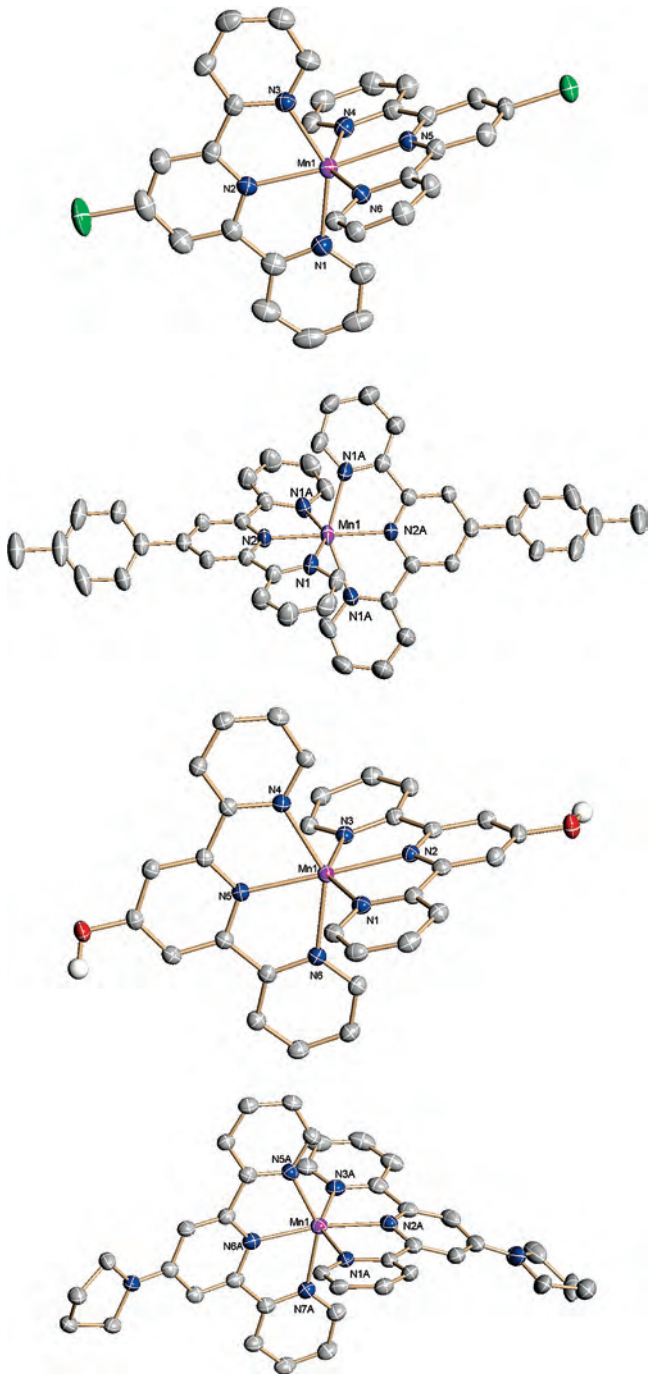

Figure 2. XSHELL representations of the $[Mn(4'\text{-X-terpy})_2]^{2+}$ cations at 50% probability level; from top to bottom: $[Mn(4'\text{-Cl-terpy})_2]^{2+}$, $[Mn(4'\text{-}CH_3Ph\text{-terpy})_2]^{2+}$, $[Mn(4'\text{-OH-terpy})_2]^{2+}$, and $[Mn(4'\text{-pyrr-terpy})_2]^{2+}$.

B3LYP functional and LANL2DZ basis-set,[23] we were able to discriminate between crystal lattice and true electronic effects (Table 2).

The geometries of the $[Mn(II)(4'\text{-X-terpy})_2](ClO_4)_2$ compounds reported here were comparable to other first row transition metal complexes with ligands from the terpy family.[26] Two ligands coordinated meridionally forming $[MnN_6]^{2+}$-type complex cations with a highly tetragonally distorted octahedral geometry (see also Table 2). This distortion is a persistent feature of all first row transitions metal complexes with terpyridine derivatives.[26] In the $[Mn(4'\text{-X-terpy})_2]^{2+}$ cations, the Mn−N distances ranged from 2.156(4) to 2.286(3) Å. The Mn−N(central) distances weakly followed the electron-donating potential of the 4′-substituent and were significantly shorter than the Mn−N(distal) bond lengths, which were essentially independent of the 4′-substituent (Table 2 and Figure 3).

The difference between the average Mn−N(distal) and Mn−N(central) bond lengths ($|(Mn-N_{distal}) - (Mn-N_{central})|$) was used as a measure of the tetragonal distortion. For $[Mn(4'\text{-Cl-terpy})_2](ClO_4)_2$ and $[Mn(4'\text{-OH-terpy})_2](ClO_4)_2$, the difference was comparable to Mn(II) complexes found in the literature,[25,27] (0.056 Å and 0.066 Å, respectively), while in the case of $[Mn(4'\text{-}CH_3Ph\text{-terpy})_2](ClO_4)_2$ and $[Mn(4'\text{-pyrr-terpy})_2](ClO_4)_2$, it amounted to 0.1 Å (0.097 Å and 0.110 Å, respectively), one of the largest seen in compounds of this type. Hence, the degree of tetragonal distortion followed the electron-donor capacity of the 4′-substitution (Cl < OH < pyrr), with $[Mn(4'\text{-pyrr-terpy})_2](ClO_4)_2$ displaying the highest degree of distortion in the solid state. The CH_3Ph-substituted complex was the only exception from this observation with a distortion comparable to that of $[Mn(4'\text{-pyrr-terpy})_2](ClO_4)_2$, in spite of its distinctly lower electron-donating power. In this case, the steric hindrance introduced by the large residue in the 4′-position likely outweighed the electronic/inductive effect in the solid state.

The variations in bond distances were also seen in B3LYP/LANL2DZ[23] geometry optimized structures (see Table 2 and Figure 3). On average, the theoretical distances were slightly longer by no more than 0.03 Å and were slightly less sensitive to the 4′-substitution when compared to the experimentally determined data. This agreement also extended to the angles $N(distal)_{L1}-Mn-N(distal)_{L2}$ which in both cases were on the average of 145°. Together, this indicated the variation in tetragonal distortion was inherent to the terpy ligand and the 4′-substitution and not due to lattice effects. The biggest differences between theoretical and crystallographic structures were seen in the angular relationship between the two ring systems. This difference is reasonable as crystal packing effects were likely to be present in the solid state. In all calculated structures, the $N(central)_{L1}-Mn-N(central)_{L2}$ angle was 180° and the ring planes were orthogonal. It is evident from Table 2 that this was not the case in the crystallographic structures. While the angle $N(central)_{L1}-Mn-N(central)_{L2}$ for the $4'\text{-}CH_3Ph$-terpy complex was exactly 180°, it deviated for the other

(26) For example, see (a) Figgis, B. N.; Kucharski, E. S.; White, A. H. *Aust. J. Chem.* **1983**, *36*, 1537−1561. (b) Baker, A. T.; Goodwin, H. A. *Aust. J. Chem.* **1985**, *38*, 207–214. (c) Folgado, J.-V.; Henke, W.; Allmann, R.; Stratemeier, H.; Beltrán-Porter, D.; Rojo, T.; Reinen, D. *Inorg. Chem.* **1990**, *29*, 2035–2042. (d) Jeitler, J. R.; Turnbull, M. M.; Wikaira, J. L. *Inorg. Chim. Acta* **2003**, *351*, 331–344. (e) McMurtrie, J.; Dance, I. *CrystEngComm* **2005**, *7*, 216–229. (f) Indumathy, R.; Radhika, S.; Kanthimathi, M.; Weyhermüller, T.; Nair, B. U. *J. Inorg. Biochem.* **2007**, *101*, 434–443.

(27) (a) Bhula, R.; Weatherburn, D. C. *Aust. J. Chem.* **1991**, *44*, 303–307. (b) Freire, E.; Baggio, S.; Garland, M. T.; Baggio, R. *Acta Crystallogr., Sect. C* **2001**, *57*, 1403–1404. (c) Rompel, A.; Bond, A. D.; McKenzie, C. J. *Acta Crystallogr., Sect. E* **2004**, *60*, m1759–m1760. (d) Baffert, C.; Romero, I.; Pécaut, J.; Llobet, A.; Deronzier, A.; Collomb, M.-N. *Inorg. Chim. Acta* **2004**, *357*, 3430–3436.

Table 2. Bond Lengths (Å) and Angles (deg) for [Mn(4′-X-terpy)$_2$] Complexes Determined by X-ray Crystallography, Listed in the Order of Decreasing Hammett Constant for the 4′-Substituent[a]

X = Hammett constant σ_{Para}[b]	Cl 0.23	H[c] 0	CH_3Ph −0.03	OH −0.37	pyrrolidine[e] −0.83
Mn−N(distal)$_{av}$	2.25(2)	2.259(2)	2.285(3)	2.260(10)	2.27(2)
	(2.278)	(2.274)	(2.278)	(2.275)	(2.280)
Mn−N(central)$_{av}$	2.194(2)	2.214(1)	2.188(4)	2.194(1)	2.160(3)
	(2.216)	(2.212)	(2.198)	(2.208)	(2.190)
N(distal)$_{L1}$−Mn−N(distal)$_{L1}$[d]	145.30(16)	144.58(19)	144.15(13)	144.45(6)	145.57(13)
					144.31(13)
N(distal)$_{L2}$−Mn−N(distal)$_{L2}$	145.84(16)	144.1(2)	144.15(13)	144.47(6)	146.08(13)
					145.56(13)
	(145.6)	(145.7)	(145.7)	(145.7)	(145.8)
N(central)$_{L1}$−Mn−N(central)$_{L2}$	173.63(16)	177.3(2)	180	177.90(6)	168.57(13)
					167.47(13)
θ, dihedral angle	87.01(3)	89.9	60.52(3)	89.51(1)	86.30(2)
					82.77(2)
	(90.0)	(90.0)	(90.0)	(89.9)	(90)

[a] As a comparison, the bond lengths and angles from the optimized B3LYP/LANL2DZ structures have been included in parenthesis below the corresponding crystallography data. [b] Data from ref 14. [c] Data from ref 25. [d] L1, ligand 1; L2, ligand 2. [e] Two independent molecules in the asymmetric unit.

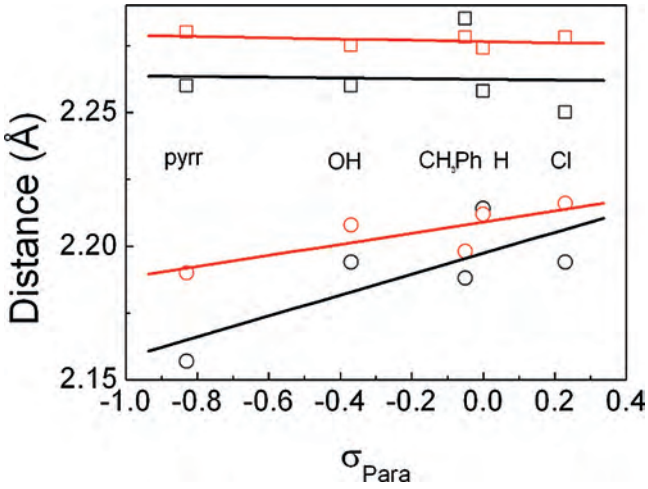

Figure 3. Comparison of the experimentally determined Mn−N distances (black) with those from the B3LYP/LANL2DZ optimized structures (red): $N_{central}$−Mn (circles) and N_{distal}−Mn (squares). Solid lines are for visual purposes only.

compounds, being the smallest for the pyrr-substituted complex; see Table 2. The 4′-OH derivative displayed an angle of 177.90(6)° which was closest to the one found in unsubstituted Mn−terpyridyl complexes.[25,27] The two terpyridine ligands were nearly orthogonal to one another in [Mn(4′-X-terpy)$_2$]$^{2+}$(X = Cl, OH, pyrr), with dihedral angles θ of 87.01(3)°, 89.51(1)°, and 86.30(2)°/82.77(2)°, respectively (two independent molecules in the case of the 4′-pyrr-derivative). This observation was in good agreement with other bis(terpyridine) complexes of transition metal ions reported in the Cambridge Structural Database (Version 5.28, θ_{av} ca. 87(2)°).[28] In contrast, this angle was 60.52(3)° in [Mn(4′-CH_3Ph-terpy)$_2$]$^{2+}$, comparable to the very small angle in the copper(II) complex of 4′-CH_3Ph-terpy (69.2°).[29] Very recently, the structure of [Mn(4′-CH_3Ph-terpy)$_2$]$^{2+}$ placed as a guest in a copper(I) pseudohalide network has been reported by Zhou et al.[30] In this case, the expected interplane angle close to 90° was observed. The lattice apparently had a large influence and contributed to a more relaxed arrangement around the metal center.

To extend our studies toward a system that was more closely related to the actual donor set found in the active site of MnSOD, we chose the ligand *N*,*N*-bis(2-ethyl-5-methyl-imidazol-4-ylmethyl)aminopropane (biap).[13] Following the same Hammett concept that we employed for the terpy-system, several derivatives of benzoic acid (Hbz) with para-substituents of varying electron-donating capacity (p-X-bz), namely, X = NO_2, Cl, H, Ph, ^{t}Bu, and CH_3, were used as coordinating counterions. The complexes [Mn(biap)(p-X-bz)$_2$(H_2O)], with X = Cl, H, CH_3, were characterized structurally by X-ray diffraction analysis; see Figure 4. In contrast to results published earlier by Reedijk and coworkers,[20] we did not observe the formation of a five-coordinate manganese center when employing benzoate as counterion. All derivatives presented here were isomorphous complexes with the manganese atom in the center of a distorted octahedron. The equatorial plane was formed by two nitrogen atoms provided by the imidazole residues of the biap ligand and two carboxylic oxygen atoms from monodentate benzoic acid ligands. The axial positions were occupied by the tertiary nitrogen atom of the biap ligand and a water molecule. The three oxygen atoms were oriented in a meridional fashion with the water molecule forming intramolecular hydrogen bonds with the carbonyl oxygen atoms of the benzoic acid molecules. Crystal structure and refinement data for all of the complexes can be found in the Supporting Information together with a listing of important bond lengths and angles. In all cases, it was difficult to assign any comparable influences related to the Hammett parameter σ_{Para} on the overall structure of the complexes as determined by X-ray crystallography.

High-frequency and high-field EPR (HFEPR) spectra of the biap complexes as powders confirmed the structural homology for all compounds (X = NO_2, Cl, H, Ph, ^{t}Bu, and CH_3) in the solid state. Frozen acetonitrile solution spectra were significantly different from powder spectra for all but one complex (X = Cl). The lability of the coordinating anions strongly suggested that the solution

(28) Allen, F. H. *Acta Crystallogr., Sect. B* **2002**, *58*, 380.
(29) Uma, V.; Vaidyanathan, V. G.; Nair, B. U. *Bull. Chem. Soc. Jpn.* **2005**, *78*, 845–850.
(30) Zhou, X.-P.; Ni, W.-X.; Zhan, S.-Z.; Ni, J.; Li, D.; Yin, Y.-G. *Inorg. Chem.* **2007**, *46*, 2345–2347.

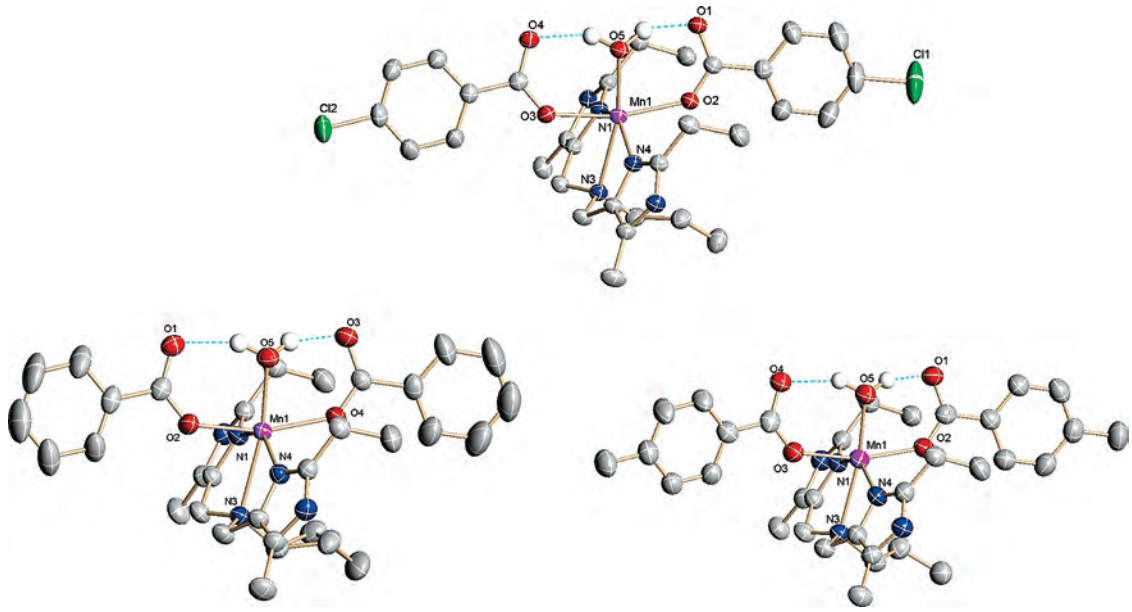

Figure 4. XSHELL representations of [Mn(biap)(p-X-bz)$_2$(H$_2$O)] at 50% probability level, hydrogen atoms were omitted for clarity (except those of H$_2$O). Top, [Mn(biap)(p-Cl-bz)$_2$(H$_2$O)]; bottom left, [Mn(biap)(bz)$_2$(H$_2$O)]; bottom right, [Mn(biap)(p-CH$_3$-bz)$_2$(H$_2$O)]; hydrogen bonds are shown in light blue.

structures were completely different from the ones observed in the solid state. This meant that we could not with any confidence relate the electrochemical measurements that were carried out in solution with the Hammett parameter σ_{Para} (see below).

The HFEPR spectra of the manganese terpy complexes as powders and in frozen solution were very instructive and critical for relating crystallographic structural data to the electrochemical measurements. In brief, we found no correlation between 4′-substitution of the Mn(4′-X-terpy)$_2$-(ClO$_4$)$_2$ complexes and the Mn(II) zero-field interaction in the powder spectra, while in the crystal structures, influences of the electronic effect of the 4′-substituent on bond lengths and angles around the metal center were observed. In contrast to the results obtained in the solid state, the zero-field interaction could be related to the electron-donating capacity of the 4′-substituent when HFEPR spectra of the complexes in frozen acetonitrile solution were examined. This indicated that lattice effects may have obscured the behavior that became apparent in solution. All HFEPR spectra are described in a recent communication.[17]

To examine the solution properties of the manganese-biap as well as the manganese and iron terpyridine complexes further, we have performed electrochemical measurements. Figure 5a−c shows typical electrochemical responses for the investigated iron terpy-complexes, exemplified by the [Fe(4′-CH$_3$Ph-terpy)$_2$]$^{2+}$voltammetry.

All of the complexes in this series gave one metal-centered Fe(II)/Fe(III) oxidation and two ligand-based reductions. The iron-centered reaction was reversible in all complexes investigated, with CV peak current ratios (i_p(Ox)/li_p(Red)l) between the oxidation and the rereduction process close to 1[31] and peak potential separations (ΔE_p) ranging between 60 and 80 mV[32] for all but the [Fe(terpy)$_2$]$^{2+}$ complex cation, where the peak separation was significantly larger, 120 mV. This complex also showed a larger absolute value for the difference in peak potential (E_p(Ox)) and half-peak potential ($E_{p\ 1/2}$(Ox)), $|E_p(Ox) - E_{p1/2}(Ox)| = 75$ mV, than the iron

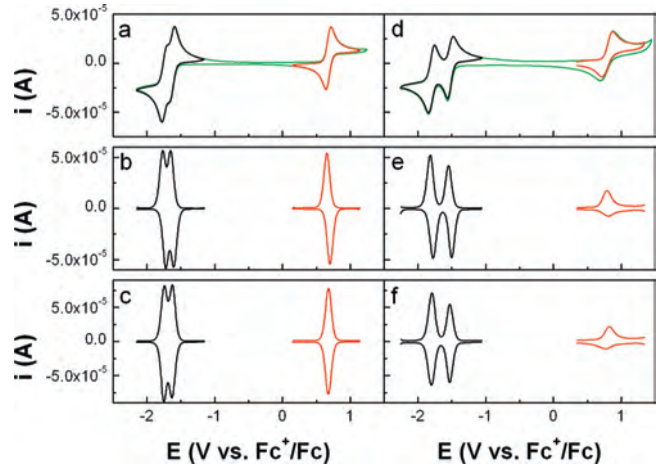

Figure 5. Electrochemical responses from [Fe(4′-CH$_3$Ph-terpy)$_2$]$^{2+}$ (a-c) and for [Mn(4′-CH$_3$Ph-terpy)$_2$]$^{2+}$ (d–f) in a 2 mM acetonitrile solution with 0.1 M TBAPF6 as supporting electrolyte. The top panels (a and d) show cyclic voltammetry (CV) at 0.1 Vs^{-1}, b and c show differential pulse (DPV) responses and the bottom panels show square wave voltammetry (SWV) responses using the conditions stated in the experimental section. All techniques gave two ligand based reductions (black) and one metal-centered oxidation (red). In green a full CV scan over the whole potential region is shown.

(31) Absolute quotients of the oxidation- and reduction peak currents (i_p(Ox)/li_p(Red)l) at a scan rate of 0.1 V s^{-1} for the respective complexes (in parenthesis) were 1.2 ([Fe(terpy)$_2$]$^{2+}$), 1.0 ([Fe(4′-Cl-terpy)$_2$]$^{2+}$), 1.0 ([Fe(4′-CH$_3$Ph-terpy)$_2$]$^{2+}$), 1.0 ([Fe(4′-OH-terpy)$_2$]$^{2+}$), 1.0 ([Fe(4′-pyrr-terpy)$_2$]$^{2+}$), 1.0 ([Fe(4′-DMA-terpy)$_2$]$^{2+}$), 0.9 ([Mn-(terpy)$_2$]$^{2+}$), 1.0 ([Mn(4′-Cl-terpy)$_2$]$^{2+}$), 1.2 ([Mn(4′-CH$_3$Ph-terpy)$_2$]$^{2+}$), 1.3 ([Mn(4′-OH-terpy)$_2$]$^{2+}$), and 1.0 ([Mn(4′-pyrr-terpy)$_2$]$^{2+}$).

(32) Peak splits between the oxidation- and the reduction peak (ΔE_p) at a scan rate of 0.1 V s^{-1} for the respective complexes (in parenthesis) were 121 mV ([Fe(terpy)$_2$]$^{2+}$), 74 mV ([Fe(4′-Cl-terpy)$_2$]$^{2+}$), 77 mV ([Fe(4′-CH$_3$Ph-terpy)$_2$]$^{2+}$), 67 mV ([Fe(4′-OH-terpy)$_2$]$^{2+}$), 76 mV ([Fe(4′-pyrr-terpy)$_2$]$^{2+}$), 71 mV ([Fe(4′-DMA-terpy)$_2$]$^{2+}$), 236 mV ([Mn(terpy)$_2$]$^{2+}$), 283 mV ([Mn(4′-Cl-terpy)$_2$]$^{2+}$), 151 mV ([Mn(4′-CH$_3$Ph-terpy)$_2$]$^{2+}$), 256 mV ([Mn(4′-OH-terpy)$_2$]$^{2+}$), and 108 mV ([Mn(4′-pyrr-terpy)$_2$]$^{2+}$).

4′-X-terpy complexes for which the corresponding values[33] were close to the 56.5 mV expected for a fully reversible reaction. Also, the differential pulse (DPV) and square wave voltammetry (SWV) responses indicated reversible Nernstian reactions for all complexes (Figure 5, panels b and c) with symmetrical peaks of comparable size for both oxidative and reductive scans. The difference in peak potential for the oxidative scan and the reductive scan was in all cases close to the expected 50 mV for DPV measurements and zero for SWV measurements, except for $[Fe(terpy)_2]^{2+}$.

A metal-centered II/III oxidation was observed for the manganese terpy complexes (Figure 5d−f), and for $[Mn(4'\text{-pyrr-terpy})_2]^{2+}$ also, the Mn(III)/Mn(IV) transition was observed at 1.12 V versus Fc^+/Fc. Compared to the corresponding iron complexes, the manganese II/III potential was shifted by 0.1–0.3 V, depending on the ligand, to higher potential (Figure 5). The electrochemical responses for this transition indicated a more complicated redox chemistry in the manganese case with large separations between the oxidation- and the re-reduction wave[32] and peak current ratios differing from 1.[31] As the scan rate was lowered (from the 0.1 V s^{-1} reported), the peak current decreased approximately with the square root of the scan rate, and the peak separation decreased slowly. The oxidation and reduction peak currents were also similar at lower scan rates. At higher scan rates (10 V s^{-1}) the peak separation increased dramatically, the linear dependence of the peak current with the square root of the scan rate was lost, and the peaks were also significantly broadened. This indicated a quasi-irreversible behavior due to slow heterogeneous electron transfer. This was likely due to the expected Jahn–Teller distortion that occurs with oxidation to Mn(III).[34] The responses from the pulsed techniques indicated non-Nernstian behavior. In all cases, the peaks for the II/III transition were broadened and smaller than expected for a Nernstian transition (Figure 5, panels e and f).

With the exception of the OH-terpy[35] based metal complexes, all terpy-complexes gave two fully reversible ligand-based reductions. In $[Mn(4'\text{-Cl-terpy})_2]^{2+}$, a third irreversible reduction was observed that was assigned to the metal center due to its absence in the corresponding iron complex. This reaction caused degradation of the electrode surface, and only first scans were used since the electrode surface had to be regenerated by polishing to reproduce the electrochemical response. The two ligand-based reductions were typically separated by some hundred millivolts. Interestingly, the separation between the two ligand reductions was systematically larger in the manganese complexes as compared to the corresponding iron complexes (compare Figure 5a−c and d−f).

Table 3. Reduction Potentials of Iron and Manganese Complexes in Acetonitrile solution with 0.1 M $TBAPF_6$ as Supporting Electrolyte versus Fc^+/Fc Evaluated from DPV Measurements[a]

complex	σ_{Para}[b]	E^0 (V vs Fc^+/Fc) Me(III)/Me(II)	reductions		
$[Fe(4'\text{-Cl-terpy})_2]^{2+}$	0.23	0.77	−1.54	−1.7	
$[Fe(terpy)_2]^{2+}$	0	0.72	−1.64	−1.81	
$[Fe(4'\text{-CH}_3\text{Ph-terpy})_2]^{2+}$	−0.03	0.68	−1.63	−1.74	
$[Fe(4'\text{-OH-terpy})_2]^{2+}$	−0.37	0.55	−1.78[c]	−1.97[c]	
$[Fe(4'\text{-pyrr-terpy})_2]^{2+}$	−0.83	0.26	−1.91	−2.05	
$[Fe(4'\text{-DMA-terpy})_2]^{2+}$	−0.83	0.28	−1.90	−2.03	
$[Mn(4'\text{-Cl-terpy})_2]^{2+}$	0.23	1.06	−1.46	−1.71[d]	−2.21
$[Mn(terpy)_2]^{2+}$	0	0.88	−1.54	−1.89	
$[Mn(4'\text{-CH}_3\text{Ph-terpy})_2]^{2+}$	−0.03	0.80	−1.52	−1.80	
$[Mn(4'\text{-OH-terpy})_2]^{2+}$	−0.37	0.71	−1.77[c]	−1.99[c]	
$[Mn(4'\text{-pyrr-terpy})_2]^{2+}$	−0.83	0.40	−1.94	−2.09	

[a] Also listed is the Hammett constant (σ_{Para}) for the respective 4′-substituent. [b] Data from ref 14. [c] Reduction potential estimated from irreversible DPV reductive scan. [d] Metal based reduction

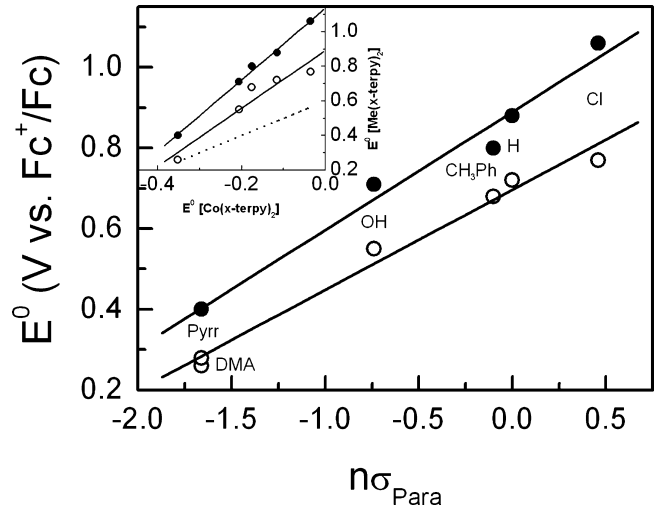

Figure 6. The reduction potential for $[Fe(4'\text{-X-terpy})_2]^{3+/2+}$ (open circles) and for $[Mn(4'\text{-X-terpy})_2]^{3+/2+}$ (closed circles) as a function of σ_{Para} for the substituent (X) times the number of substituents ($n = 2$). Solid lines represent best fits of the data. The inset shows the same data as a function of the reduction potential for the corresponding cobalt complex (for $[Co(4'\text{-X-terpy})_2]^{2+}$) taken from ref 16c. A dotted line of slope 1 representing the cobalt dependence on the substituent is also included in the graph.

Table 3 lists the reduction potentials evaluated from the electrochemical measurements. Also included in the table are the Hammett constants (σ_{Para}) for the relevant substituents.[14] As stated in the introduction, this parameter measures the electron-donating/electron-withdrawing properties of the substituent. There was a strong correlation between reduction potential and both metal-centered and ligand-centered reactions as seen in Figure 6, where the reduction potential for the metal-centered reaction is plotted against the Hammett constants σ_{Para} times the number of substituents ($n = 2$).

Clearly, there is a linear correlation between reduction potential and Hammett parameter with the manganese complexes being slightly more affected by the ligand substitution compared to the iron analogues. The reaction constant ρ, which is a measure of the influence that the substituent has on the metal redox chemistry, was evaluated

(33) Absolute values of the separation between the peak potential and the half-peak potential $|E_p(Ox) - E_{p1/2}(Ox)|$ at a scan rate of 0.1 V s^{-1} for the respective complexes (in parenthesis) were 73 mV-($[Fe(terpy)_2]^{2+}$), 61 mV ($[Fe(4'\text{-Cl-terpy})_2]^{2+}$), 62 mV ($[Fe(4'\text{-CH}_3\text{Ph-terpy})_2]^{2+}$), 57 mV ($[Fe(4'\text{-OH-terpy})_2]^{2+}$), 61 mV ($[Fe(4'\text{-pyrr-terpy})_2]^{2+}$), 59 mV ($[Fe(4'\text{-DMA-terpy})_2]^{2+}$), 107 mV ($[Mn(terpy)_2]^{2+}$), 123 mV ($[Mn(4'\text{-Cl-terpy})_2]^{2+}$), 79 mV ($[Mn(4'\text{-CH}_3\text{Ph-terpy})_2]^{2+}$), 109 mV ($[Mn(4'\text{-OH-terpy})_2]^{2+}$), and 69 mV ($[Mn(4'\text{-pyrr-terpy})_2]^{2+}$).

(34) Huheey, J. E. *Inorganic Chemistry: Principles of Structure and Reactivity*, 3rd ed.; Harper & Row: New York, 1983.

(35) For $[Mn(OH\text{-terpy})_2]^{2+}$ and $[Fe(OH\text{-terpy})_2]^{2+}$,two ligand reductions were observed, but they produced no reoxidation peak on scan reversal. For the iron complex, the response was reproducible on consecutive scans, while reduction of the manganese complex caused degradation of the electrode surface.

Table 4. Reaction Constants (ρ) for Terpy-Complexes with Varying Substituents in 4′-Position for Different Central Metals and Peak Separation between the Ligand-Centered Reductions (ΔE^0)

complex series	ρ	ΔE^0 reduction [mV]
$[Mn(4'\text{-X-terpy})_2]^{2+}$	5.0	350
$[Fe(4'\text{-X-terpy})_2]^{2+}$	4.2	170
$[Co(4'\text{-X-terpy})_2]^{2+}$	2.4[a]	–
$[Os(pyterpy)_2]^{2+}$	4.7[b]	320[b]
$[Ru(pyterpy)_2]^{2+}$	4.0[b]	250[b]
$[Fe(pyterpy)_2]^{2+}$	3.7[b]	180[b]

[a] Data from ref 16c. [b] Data from refs 16a and 31.

from the slope of the linear fit by dividing by $-RT/F$ (-59.2 mV). The resulting values for the constant ρ are listed in Table 4 together with literature data for the corresponding cobalt complexes[16c] and for a similar set of terpy-based metal complexes with iron, ruthenium, and osmium as central metal.[16a,36]

In the Mn(biap)(p-X-bz)$_2$-type complexes, no ligand-based reactions were observed. The voltammetry showed one oxidation peak. However, when the scan was reversed, two re-reduction peaks were found that were separated from the oxidation peak by almost 1 V. In these complexes, the reduction potential, as evaluated from the forward DPV-scan, increased as the Hammett constant increased (data not shown). The effect of the substitution was, however, much less pronounced than in the case of the terpy complexes. This nonideal behavior was not unexpected given the fact that the HFEPR from frozen solution were significantly different from the powder spectra. This made further interpretation of the results difficult.

Although correlations between Hammett constants and redox potential were gratifying, we had no detailed understanding of how the substituents affected the electronic structure at the molecular level, notably how the substituents affected the charge distribution. To this end, we carried out density functional calculations to determine charge and spin distributions.[23] For both the biap complexes and the terpy-derivatives, we were able to relate the electron-donating capacity of the substituents charge on the ligating atom.[17] The charge on the central nitrogen on the terpy derivatives, determined from a Natural Bond Order (NBO) analysis, increased monotonically with the Hammett constant of the substituent for the Mn(4′-X-terpy)$_2$-series spanning a range of 0.06 charge units, while the charge on the manganese was less affected and showed a more complex behavior spanning less than 0.02 charge units (Figure 7). In comparison to the Mn complexes, the substituent effect on the iron terpy system appeared to be slightly attenuated. Both the nitrogen and the iron NBO charges monotonically raised with increasing Hammett constants with a span of only 0.03 both for metal and nitrogens (Figure 7). Hence, as was the case with the redox potential measurements, the iron complexes appear to be slightly less sensitive to substituent effects than manganese. These density functional calculations showed that Hammett constants were indeed a relevant quantitative measure of the effect of the substituents on charge distribution and that the observed correlation with redox potentials was rooted in the electron-donating/withdrawing capacities of the substituents.

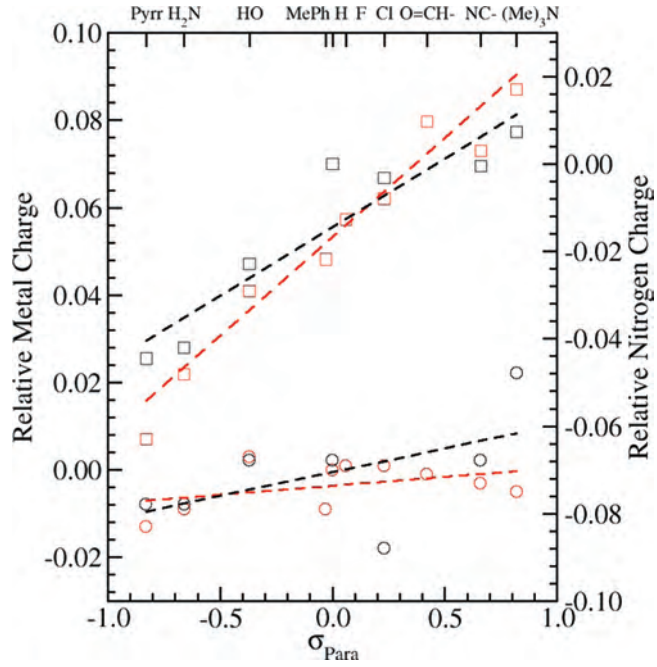

Figure 7. B3LYP/6-311G Natural Bond Orbital charges for the Me(4′-X-terpy)$_2$-series as a function of the Hammett constants. The circles denote the metal charges, Mn in red and Fe in black, and the squares the central nitrogen charges of the Mn complexes in red and of Fe complexes in black. In each case, the charges shown are relative to the corresponding X = H complexes which in the manganese case had a metal charge of 1.67 and central nitrogen charge of -0.59 and in the iron case 1.19 and -0.51, respectively. The dashed lines are the linear regression fits of the data (manganese in red and iron in black).

Discussion

There is a growing body of knowledge that demonstrates that ring substituents on polypyridal ligands affect the reduction potential of metal–ligand systems in a linear manner when measured relative to the Hammett constant σ of the substituents. For example, the recent study of Chambers and co-workers[16c] on the 4′-substituted Fe− and Co−terpy complexes demonstrated that the reduction potentials of these complexes depended linearly on the Hammett constant σ_{Para} of the 4′-substitutent. Taken together, this property is general, covering the 4′-substituted terpy complexes of the iron group (Fe, Ru, and Os),[36] as well as those of manganese and cobalt, the principal difference being the sensitivity to substitution, that is, the slope of the linear dependence or the Hammett reaction constant ρ (Table 4).

As shown in Figure 8, this dependence of the redox properties of a metal complex on the electron-donating/withdrawing strength of a ligand apparently extends to other types of ligands with different ligating atoms and, in the case of manganese, to other oxidation states as well (for example, see ref 16b). On the basis of these observations, one would expect similar effects in proteins. Thus, simple model systems, such as metal terpy complexes, should provide an ideal paradigm for testing various aspects of the metal selective activity of superoxide dismutases. But, before doing

(36) Constable, E. C.; Cargill Thompson, A. M. W. *J. Chem. Soc., Dalton Trans.* **1994**, 1409–1418.

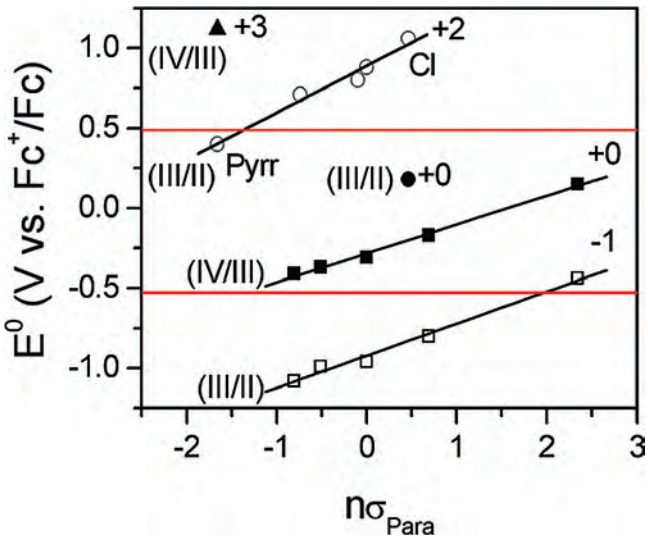

Figure 8. The reduction potential for our $[Mn(4'\text{-X-terpy})_2]^{3+/2+}$ (open circles), $Mn(biap)(p\text{-Cl-bz})_2$ (solid circle) and $[Mn(4'\text{-X-terpy})_2]^{4+/3+}$ (triangle) together with literature data from Lewis et al. 2001[16b] for a series of neutral- (solid squares) and negatively charged (open squares) manganese complex ions as a function of the Hammett constants for the substituent (X) times the number of substituents (n). Solid, black lines represent linear best fits of the data. The upper and lower red horizontal line represent the reduction potential for the one-electron reduction and oxidation of superoxide respectively. Roman numerals refer to manganese redox couple and the Arabic numbers to the charge of the complex in the reduced state.

so, it was important to have a more quantitative understanding about the origins of this ligand-dependent property that appears to be both periodic and robust to difference in spin-state and details of geometry.

The inset of Figure 6 shows the relationship between the reduction potentials for the iron− and the manganese−terpy complexes and those of their cobalt analogues. This representation had the advantage that it eliminated any uncertainty associated with the Hammett constants. A line with unity slope was included in this graph to represent the substituent effect for the cobalt complexes. Evidently, the slopes, and hence the reaction constants, are different for the different metals with manganese being somewhat more influenced by the nature of the substituent than iron. The cobalt series was the least affected. Chambers and co-workers[16c] interpreted this difference in sensitivity between the iron and the cobalt complexes as an effect of "greater inductive influence on the iron center" correlating this to the stronger metal terpyridine binding to iron as compared to cobalt. While this may be true for the iron complexes, the density-functional calculations did not support this for the manganese ones. They showed that the manganese charge was essentially constant as a function of σ_{Para}, varying only by about 1%, while the charge on the central terpy nitrogen atom varied by 13%. For the iron complexes, the charge on the same nitrogen atom changed by 10% as a function of the 4′-substitution and for the iron atom by no more than 2%. Hence, the differential sensitivity of reduction potentials of Mn and Fe complexes appeared to be more a function of the variation in central nitrogen charge rather than that of the metal ion indicating that a purely through-bond inductive mechanism was unlikely.

Simple electrostatics provided a simpler and more consistent explanation of the differential sensitivity of the reduction potential of the metal terpy complexes to 4′-substitution. A point charge mechanism would predict the iron complexes to be the most sensitive to substitution effects, because of the shortest metal−N(central) distances. Since this was not the case, such a mechanism could be readily excluded. However, the periodic trends within the Fe group and between Mn, Fe, and Co did follow the expected trends in polarizability.[37] This was also supported by the measured ligand reduction potentials. In general, it is expected that the more polarizable the metal is, the stronger the interaction between the two ligands will be. The separation between the two ligand reduction potentials (Table 4) appeared to be correlated with the metal polarizability. In general, in a molecule containing two identical, noninteracting redox centers, the reduction potentials for the two redox-centers are separated by $(RT/F)\ln 4$ for statistical reasons.[38] A larger separation, as found for the two ligand reductions in the terpy complexes indicates interactions between the two groups, mediated by the central metal ion. Reduction of the first ligand polarizes the central metal, thereby stabilizing the reduced form of the ligand. Upon reduction of the second ligand, this charge stabilization is lost since the metal is now in a symmetrical electric field. One would thus expect the more polarizable ion to give larger ligand peak separations, due to its better ability to stabilize the negative charge on the ligand. In contrast, a purely point charge interaction model for the interaction between the ligands would predict that the separation between the ligand reduction potentials would be larger for the iron than the manganese, the latter having shorter metal−nitrogen bond distances. Thus, it appears that the reaction constants per substituent *and* the ligand peak separation are correlated with increased polarizability of the central metal. Metal ion polarizability accommodates not only Mn(II) and Fe(II) terpy redox potentials, but also cobalt[16c] and the rest of the iron-group[36] in the periodic table as well.

Although the identity of the metal ion plays a defining role in determining the sensitivity of the redox potential to the electron-donating/withdrawing properties of the ligand, the dominant factor controlling the reduction potential of a manganese center was apparently the overall charge of the complex ion. This is demonstrated in Figure 8 where the reduction potentials for the metal-centered oxidation for the manganese(II) complexes investigated in this study are plotted against the total Hammett constants together with literature data for two sets of neutral (solid squares) and negatively charged (open squares) manganese complex ions.[16b] Since the $Mn(II)(4'\text{-X-terpy})_2$ complex ions (open circles) have an overall charge of 2, they constitute the high charge part of the series. In addition, the III/VI transition in $[Mn(4'\text{-pyrr-terpy})_2]^{2+}$ (solid triangle) and the $Mn(biap)(p\text{-Cl-bz})_2$ (solid circle) add one point each to this figure, representing manganese complexes (complex

(37) Pearson, R. G. *Inorg. Chem.* **1988**, *27*, 734–740.
(38) Flanagan, J. B.; Margel, S.; Bard, A. J.; Anson, F.C. J. *Am. Chem. Soc.* **1978**, *100*, 4248–4253.

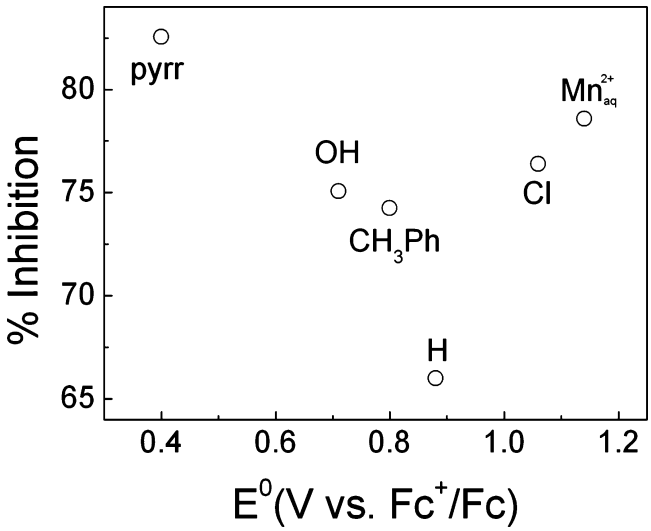

Figure 9. Inhibition of the rate of XTT reduction in a 2 μM aqueous solution of the Mn(4′-X-terpy)$_2$-complexes and of $(Mn^{2+})_{aq}$ as a function of their respective reduction potential in acetonitrile

ions) with a net charge of 3 and of 0, respectively. In a simple Coulombic model where the added electron in the reduction is treated as a point charge centered in a uniformly charged sphere, representing the metal complex, a linear increase in potential with the net charge of the complex is expected.[39] Although oversimplified, the model does account for the general trend and the order of magnitude of the effect, with close to evenly spaced steps per added net complex charge. For example, a uniformly charged sphere with a radius of 6 Å, the approximate molecular radius of the core of the terpy complexes, with a relative dielectric constant of 4 requires 600 mV per charge added.[39] Such an electrostatic contribution would be independent of the metal ion involved.

As can be seen from our data, this net-charge effect of 0.6 V per unit charge can be offset by the ligand substituent effect. This had a particularly interesting consequence for the doubly charged Mn(II)terpy complex ions of which all but one had reduction potentials too high to be thermodynamically competent to catalyze the superoxide dismutation reaction. The electron-donating capacity of the 4′-pyrrolidine substituent was so strong that it was equivalent to changing the net-charge of the complex by one charge. It sufficiently lowered the reduction potential of the complex so as to achieve the thermodynamic requirement to catalyze the dismutation reaction. We therefore tested the "activity" of the 4′-pyrrolidine substituted and the other Mn(II)(4′-X-terpy)$_2$-complexes using the standard Xanthine Oxidase/XTT assay to measure SOD protein activity.[40]

The activity (as measured in % inhibition) of the [Mn(4′-X-terpy)$_2$]-complexes followed the measured reduction potential and consequently the Hammett constant of the substituent (Figure 9). The $[Mn(4'\text{-pyrr-terpy})_2]^{2+}$ displayed the highest activity as expected from our measurements. As the reduction potential increased, the SOD activity decreased to a minimum for $[Mn(terpy)_2]^{2+}$. This trend, though pleasing, did not extend to the 4′-Cl-substituent that was the most electron-withdrawing. Along with the free Mn(II) ion, it had a higher activity than the 4′-H and 4′-CH_3Ph complexes, although it should not be thermodynamically competent with respect to the reduction potential (Table 3). This indicated that the reaction mechanism was probably not a simple electron-transfer process. More surprising was that the equivalent iron complexes that were all predicted to be thermodynamically competent showed no activity, suggesting possible kinetic limitation inherent to the assay. Nonetheless, our observation that the superoxide disproportionation activities of the Mn(II)terpy complexes did qualitatively follow a Hammett relationship is intriguing and will require a complete mechanistic study as it might have important consequences for constructing a biomimetic complex.

There are several other lessons learned from our study that have direct implications to electrochemistry and metal-specific activity of manganese and iron SODs. To achieve 600 mV change in reduction potential, large changes in electron-donating/withdrawing properties of the ligands to a Mn(II) center are required. Given the structural homology of the SOD active site and the weak nature of electrostatic interactions (for example, hydrogen-bonds) surrounding the metal center, it did not seem possible that the metal-specific activity originates from the immediate primary and secondary ligand spheres. However, it is important to appreciate that based on simple electrostatic considerations a change of 100 mV in reduction potential can be induced by a single point charge as far away as 14 Å (assuming a dielectric constant $\epsilon_r = 10$).[39] We have carried out some preliminary calculations using the continuum electrostatics/molecular mechanics program MCCE[41] in an attempt to determine whether the global or distant contributions to the electrostatic environment of the metal centers in iron and manganese SODs were the source of metal discrimination, but this was not apparent. Noodleman and co-workers have been able to correctly predict the ordering of redox potentials for *Thermus thermophilus*, human wild-type, and human Q143N mutant SODs using combined DFT and electrostatic calculations.[42] Such a combination of techniques may be needed to identify the contributions controlling the metal-specific redox potential. Within the limitations of initial calculations, local contributions appear unlikely to be sufficient, but more distant electrostatic influences to redox tuning required by the Miller−Vance model for metal-specific activity remain unidentified.

Yikilmaz and co-workers have suggested that another mechanism for redox tuning might be the modulation of the hydrogen-bond between the axial water ligand and the nearby Gln.[43–45] In this model, the strength of this interaction would

(39) Edsall, J. T.; Wyman, J. *Biophysical Chemistry, Volume 1, Thermodynamics, Electrostatics, and the Biological Significance of the Properties of Matter*; Academic Press: New York, 1958.

(40) Crapo, J. D.; McCord, J. M.; Fridovich, I. *Methods Enzymol.* **1978**, *53*, 382–393.

(41) (a) Georgescu, R. E.; Alexov, E. G.; Gunner, M. R. *Biophys. J.* **2002**, *83*, 1731–1748. (b) Alexov, E.; Gunner, M. R. *Biophys. J.* **1997**, *72*, 2075–2093.

(42) Noodleman, L.; Han, W.-G. *J. Biol. Inorg. Chem.* **2006**, *11*, 674–694.

polarize the charge of the axial ligand in much the same way as the para-substituents in our terpy complexes. In particular, Yikilmaz has argued that in MnSODs the hydrogen-bond is stronger than in FeSODs, making the axial solvent molecule more negative, thereby depressing the reduction potential of MnSOD relative to the Mn reconstituted FeSODs which would account for the metal-specific activity.[43] The results of our study would appear to support such a proposal. However, it is not clear that a charge polarization mechanism of this type would be sufficient, and studies on complexes such as the BIAP that possess a water ligand are required.

Finally, our results show that cambialism can in principle be achieved with a single ligand set, while a slightly different set can be metal-discriminating. This was demonstrated by the fact that 4′-pyrrolidine-substituted terpyridine complexes of both manganese and iron had the prerequisite reduction potential for SOD activity, while for the unsubstituted (X = H) complexes, only the iron derivative was thermodynamically competent. Moreover, since the net-charge of active site manganese and iron SODs are likely to be either +1 or 0,[10] Figure 8 suggests that the primary ligand sphere in Fe and MnSODs should render both metal ions thermodynamically competent to carry out the enzymatic reaction and, hence, is intrinsically cambialistic. As just argued, it is the more distant electrostatic contributions that may be the source of metal-specific activity.

Acknowledgment. This project was supported by a Marie Curie Intra-European Fellowships within the sixth European Community Framework Program (EIF-009546), and the Swedish Research Council. J.G. thanks the Alexander von Humboldt Foundation for a Feodor Lynen research fellowship and L.C.T., the CEA for a postdoctoral grant. V.L.P. acknowledges the National Institutes of Health for financial support (GM39406).

Supporting Information Available: Crystallographic data in CIF format and additional tables and figures. Detailed description of synthesis of the complexes and the crystallography. This material is available free of charge via the Internet at http://pubs.acs.org.

IC702428S

(43) Yikilmaz, E.; Xie, J.; Brunold, T. C.; Miller, A.-F. *J. Am. Chem. Soc.* **2002**, *124*, 3482–3483.
(44) Yikilmaz, E.; Rodgers, D. W.; Miller, A.-F. *Biochemistry* **2006**, *45*, 1151–1161.
(45) Yikilmaz, E.; Porta, J.; Grove, L. E.; Vahedi-Faridi, A.; Bronshteyn, Y.; Brunold, T. C.; Borgstahl, G. E.; Miller, A.-F. *J. Am. Chem. Soc.* **2007**, *129*, 9927–9940.